Science of the Total Environment 636 (2018) 152–167

Contents lists available at ScienceDirect

Science of the Total Environment

journal homepage: www.elsevier.com/locate/scitotenv

Urbanization and climate change implications in flood risk management: Developing an efficient decision support system for flood susceptibility mapping

Shereif H. Mahmoud *, Thian Yew Gan

Department of Civil and Environment Engineering, University of Alberta, Edmonton, Alberta T6G 1H9, Canada

HIGHLIGHTS

- Investigating climate change implication in flood risk in arid regions
- Investigating rapid urbanization implication in flood risk
- Runoff curve number method to develop surface runoff between 1948 and 2014
- Illustrate the influence of urbanization rate in surface runoff through change point trend detection
- Develop susceptibility model to delineate flood susceptibility zones

GRAPHICAL ABSTRACT

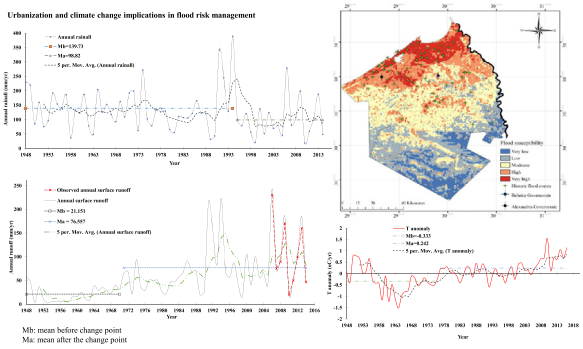

ARTICLE INFO

Article history:
Received 15 January 2018
Received in revised form 15 March 2018
Accepted 20 April 2018
Available online 26 April 2018

Editor: R Ludwig

Keywords:
Urbanization
Climate change
Surface runoff
Decision support system
Flood susceptibility

ABSTRACT

The effects of urbanization and climate change impact to the flood risk of two governorates in Egypt were analyzed. Non-parametric change point and trend detection algorithms were applied to the annual rainfall, rainfall anomaly, and temperature anomaly of both study sites. Next, change points and trends of the annual and monthly surface runoff data generated by the Curve Number method over 1948–2014 were also analyzed to detect the effects of urbanization on the surface runoff. Lastly, a GIS decision support system was developed to delineate flood susceptibility zones for the two governorates. The significant decline in annual rainfall and rainfall anomaly after 1994 at 8.96 and 15.3 mm/decade respectively was likely due to climate change impact, especially significant warming trend since 1976 at 0.16 °C/decade, though that could partly be attributed to rapid urbanization. Since 1970, effects of urbanization to flood risk are clear, because despite a decline in rainfall, the annual surface runoff and runoff anomaly show positive trends of 12.7 and of 14.39 mm/decade, respectively. Eleven flood contributing factors have been identified and used in mapping flood susceptibility zones of both sites. In the El-Beheira governorate, 9.2%, 17.9%, 32.3%, 28.3% and 12.3% of its area are categorized as very high, high, moderate, low and very low susceptibility to flooding, respectively. Similarly, in Alexandria governorate, 15.9%, 33.5%, 41%, 8.8% and 0.8% of its area are categorized as very high, high, moderate, low and very low susceptibility to flooding, respectively. Very high and high susceptible zones are located in the northern, northwestern and northeastern parts of the Beheira governorates, and in the northeastern and northwestern parts of Alexandria. The flood related information obtained in this study will be useful to assist mitigating potential flood damages and future land use planning of both governorates of Egypt.

© 2018 Elsevier B.V. All rights reserved.

* Corresponding author.
E-mail address: shereif@ualberta.ca (S.H. Mahmoud).

https://doi.org/10.1016/j.scitotenv.2018.04.282
0048-9697/© 2018 Elsevier B.V. All rights reserved.

1. Introduction

In recent years, because of urbanization, there is an increase in flood risk even in arid regions with a limited amount of annual rainfall. Various flood risk studies reported the effect of urbanization in surface runoff (Satterthwaite, 2008; Zhang et al., 2008a; Fernández and Lutz, 2010). These studies reported that increase in urban areas and impervious surfaces have led to an increase in surface runoff because less water is lost by soil infiltration. On the other hand, there are studies that attributed the rising frequency of flood occurrences to the impact of climate change (Gizaw and Gan, 2015; Jiang et al., 2015). Precipitation in arid regions tends to be more variable in time than in humid regions (Pilgrim et al., 1988), and so are more vulnerable to hydrologic extremes such as flood and droughts. In the driest continent of Africa, climate change has been linked to more frequent occurrences of severe droughts, rising temperature and altered precipitation patterns (Ramanathan et al., 2001; Shanahan et al., 2009; Williams and Funk, 2011). In countries such as Egypt, floods have been occurring more frequently and in greater severity in recent decades. A hypothesis is herein investigated, whether increasing flood events in Egypt are due to rapid urbanization or the effect of climate change.

Therefore, we will investigate the implications of urbanization and climate change in the flood risk of Egypt, which is representative of the climate of other arid regions in the Middle East. The recurrent occurrences of flooding in Egypt, especially in its coastal regions have led to catastrophic and costly damage to properties and threat to human life, which may be because of rapid urbanization along the Nile River. In northern, coastal regions of Egypt's Nile Delta and coastal areas along the Mediterranean Sea, flood discharge from wadi basins can be a threat to coastal cities, towns, and villages. Since 1990, more than seven hundred people in Egypt had lost their life because of flash floods, and about 250,000 people were affected (Guha-Sapir et al., 2014). Therefore, flood-susceptible areas should be identified so that responses to flooding emergencies can be executed quickly and effectively. Historically, Egypt's most affected regions are El-Beheira, Alexandria, Sinai, Matruh, Cairo, and Giza, which are vulnerable to the potential threat of increased surface runoff, particularly in arid regions where people tend to be ill-prepared against flood hazards.

An analysis of long-term surface runoff data of urban areas can generally reveal the effects of urbanization. A limited number of studies have used the runoff curve number method to compute surface runoff and its effects to urban communities (Lim et al., 2006; Shi et al., 2007; Banasik et al., 2014). However, most studies have not considered the effects of both urbanization and climate change impact to urban surface runoff and the development of flood susceptibility maps, e.g., (Cherqui et al., 2015; Chen et al., 2015; Xiao et al., 2017; Hong et al., 2017; Termeh et al., 2018; Zhao et al., 2018). Methods such as Multi-criteria decision support system and analytic hierarchy process have proven to be effective tools in developing flood susceptibility maps (Ouma and Tateishi, 2014; Kazakis et al., 2015; Melesse and Abtew, 2016). Researchers have used various hydrologic and climatic data that contribute to floodings, such as precipitation, runoff, digital elevation model (DEM), curvature, geology, land use/cover (urbanization), soil type, topographic wetness index and slope (Şen, 2004; Nouh, 2006). However, because of a lack of data, only a limited number of studies have used comprehensive datasets in delineating flood-prone areas of river basins. For instance, Fernández and Lutz (2010) used five flood contributing factors to analyze flood-prone areas in the Tucumán Province of Argentina: distance to the drainage channels, topography, groundwater table depths, and land use. Kazakis et al. (2015) mapped flood hazard areas of the Rhodope–Evros region of Greece based on seven factors, namely, flow accumulation, distance from the drainage network, elevation, land use, rainfall intensity and geology. Tehrany et al. (2015) did that for Malaysia using ten factors: altitude, slope, curvature, stream power index (SPI), topographic wetness index (TWI), distance from the river, geology, land use/cover (LULC), soil, and annual surface runoff, but they used a different set of factors in an earlier study (Tehrany et al., 2013).

We expect that a systematic analysis of a comprehensive dataset will lead to a representative delineation of flood susceptibility areas, which can later be validated against ground observations of past flood events. Elkhrachy (2015) used an AHP approach to map flood hazards zones in Najran city of Saudi Arabia. Among the conditions considered, annual surface runoff, soil type, surface slope, surface roughness, drainage density, distance to the main channel and land use, Elkhrachy (2015) assigned a weighting factor of 35.5% to the annual surface runoff, making it one of the most important factors in flood susceptibility mapping. Many past studies derived the relative contribution of each factor to floods based on authors' experience, literature review and weighting methods and validate final flood susceptibility maps developed against historical flood records. Flash floods occur periodically in El-Beheira and Alexandria governorates due to a lack of proper drainage systems and rapid urbanization. In 2013, surface runoff destroyed about 121 km^2 of agricultural land in El-Beheira governorate. Alexandria governorate also suffered from increased surface runoff that badly flooded streets of the coastal city and damaged many private properties. Residents of Alexandria expressed their outrage at the former government of Alexandria that failed to efficiently flood-proof the city against foreseeable events. In recent years, floods in El-Beheira had caused twenty-five deaths, forced hundreds of schools to shut down, dozens of people were forced to evacuate from their homes, and large swathes of buildings in the region were destroyed. Therefore, the objective of this study was to investigate the effects of urbanization and climate change in the flood risk management of arid regions, in addition, to developing flood susceptibility maps to support decision making in the rescue operation.

To achieve our objectives, we first analyzed the variability and trends of the annual precipitation and temperature of the two governorates to estimate the possible impact of climate change. Next, to estimate the effects of urbanization to the flood risk of the two governorates, we applied the runoff curve number method to develop the time series of surface runoff for the two governorates between 1948 and 2014. Change point detections and trend analysis techniques were then applied to the surface runoff data to find the change points and trend. Surface runoff anomalies were also analyzed to assess the influence of urbanization in surface runoff. Finally, we developed a GIS decision support system to delineate flood susceptibility zones in the Beheira and Alexandria governorates of Egypt. The accuracy of the flood susceptibility maps developed was verified with historical flood records.

This study is necessary given there is generally a lack of flood susceptibility maps in Egypt and information related to the influence of climate change and urbanization in the surface runoff of Egypt. Similar situations are found in many if not all Middle Eastern countries of arid climate. Other than useful for flood risk management, flood susceptibility maps we have developed will also benefit planners and governments in choosing suitable locations for future developments and in mitigating potential flood damages and future land use planning in Beheira and Alexandria governorates. Furthermore, the surface runoff time series developed could be used in other hydrological studies in the two governorates of Egypt.

2. Study area

This study was conducted in two governorates of Egypt. The first is the El-Beheira governorate (Fig. 1) is located in the north coastal region of Egypt's Nile Delta (30.61°N, 30.43°E) with an area of about 10,130 km^2. El-Beheira's annual rainfall ranges from 29 mm/year in the south to 190 mm/yr in the north. The second is the Alexandria governorate (31.20°N, 29.92°E) which lies along the Mediterranean coast, at about 70 km northwest of the Nile Delta (Fig. 1) occupying an area of 2818 km^2 and an average annual rainfall of about 169 mm/yr.

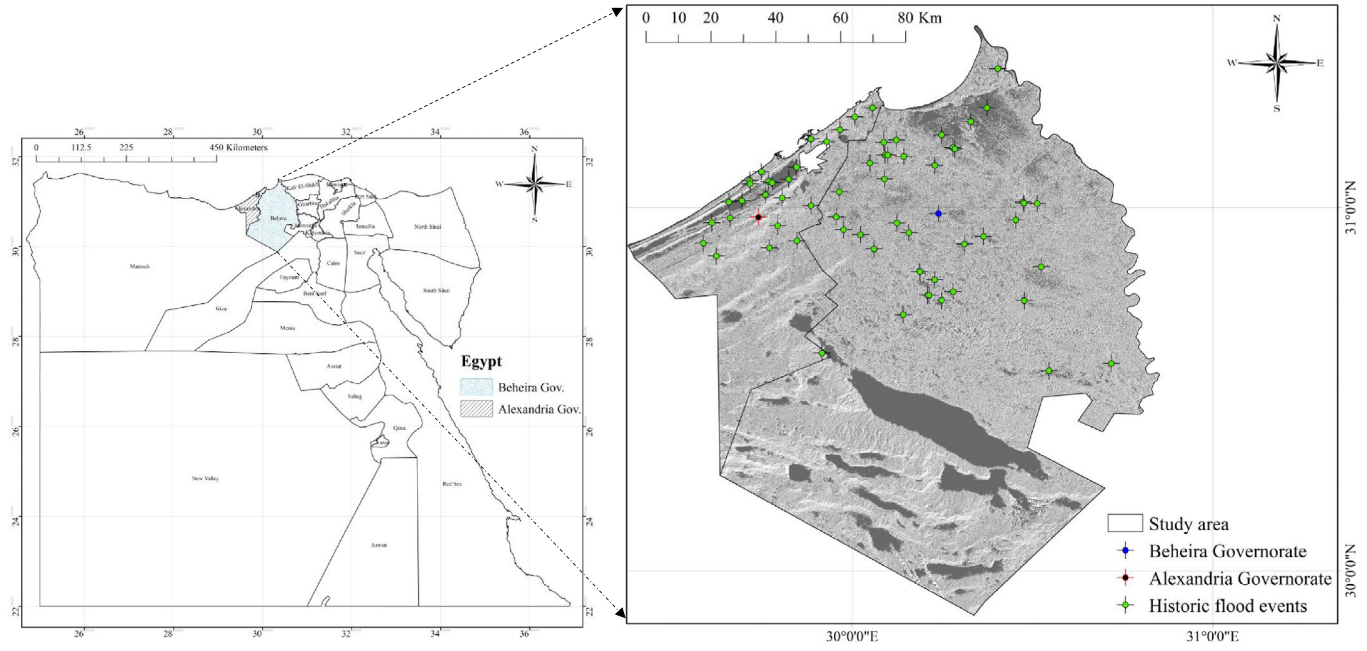

Fig. 1. Location of Beheira and Alexandria governorates in Egypt.

Alexandria's rainfall predominantly occurs along the north coastal area, which is heavily urbanized, and it decreases quickly southwards.

3. Materials and methods

3.1. Climate change detection

Long-term monthly rainfall and temperature data between 1948 and 2014 were obtained from the University of Delaware and processed to derive mean annual temperature and rainfall, rainfall and temperature anomalies between 1948 and 2014. We applied two nonparametric, change point detection methods, SNHT and Buishand's methods to mean monthly rainfall, annual rainfall, and rainfall anomaly data. We also conducted trend analysis on temperature data to detect warming trends which has been attributed to rising concentration of greenhouse gases caused by anthropogenic activities (Ren et al., 2008; Yan et al., 2010; Banasik et al., 2014). The SNHT test has been commonly used to detect a shift in the mean value of climate time-series (Wijngaard et al., 2003; Wang et al., 2007; Zhang et al., 2008b). The test check for a null hypothesis (no change point or trend) and an alternative hypothesis, where the time series tested may have a change point or a trend, or both:

$$M_x = x\overline{Z}_1 + (n-x)\overline{Z}_2 \tag{1}$$

where x = 1, 2, 3…, n.

M_x is a statistic to compute the mean temperature/rainfall value at year x with the mean value at year n-x.

Where $\overline{Z}_1 = \frac{1}{x}\sum_{i=1}^{n}\frac{(x_i-\overline{x})}{s}$ and $\overline{Z}_2 = \frac{1}{n-x}\sum_{i=x+1}^{n}\frac{(x_i-\overline{x})}{s}$.

Where s is the number of positive minus the number of negative differences between x_{i+1} and x_i, $(x_{i+1}-x_i)$, $i = 1, 2\ldots, n-1$. If s is positive, $x_{i+1} > x_i$, and if s is negative, then $x_{i+1} < x_i$. The year x is considered as a change point if the value of M_x is maximum. To reject the null hypothesis the following statistic should be achieved; the value of T_0 should be greater than the critical value of the test.

$$T_0 = \max_{1\le x\le n} M_x \tag{2}$$

Buishand's method works in a similar manner but instead on comparing the mean at each year to the critical value, the test uses the adjusted partial sum defined as:

$$Sum_0 = 0 \tag{3}$$

$$Sum_x = \sum_{i=1}^{x}(x_i-\overline{x}) \tag{4}$$

If $Sum_0 = 0$, the time series is homogeneous, and we accept the null hypothesis. However, if Sum_x is maximum or minimum which means there is a change point at year x. The magnitude of Sum_x indicates the type of shift in the time series such that a maximum value indicates a downward shift and a minimum value indicates upward shift. The adjusted range, A is as follow:

$$A = \frac{\left(\max_{0\le x\le n} Sum_x - \min_{0\le x\le n} Sum_x\right)}{S} \tag{5}$$

where $A/\sqrt{n}$ is then compared with the critical values of the test according to Buishand (1982), to check if the change point is statistically significant.

Then, the non-parametric Mann–Kendall was used to detect trend in temperature anomalies and monthly, annual and anomaly rainfall time series between 1948 and 2014:

$$S = \sum_{i=1}^{n-1}\sum_{j=i+1}^{n} sgn(x_j-x_i) \tag{6}$$

Each data point x_i is considered as a reference and compared with the remaining data points x_j:

$$Sgn(x_j-x_i) = \begin{cases} +1 & if\ (x_j-x_i)>0 \\ 0 & if\ (x_j-x_i)=0 \\ -1 & if\ (x_j-x_i)<0 \end{cases} \tag{7}$$

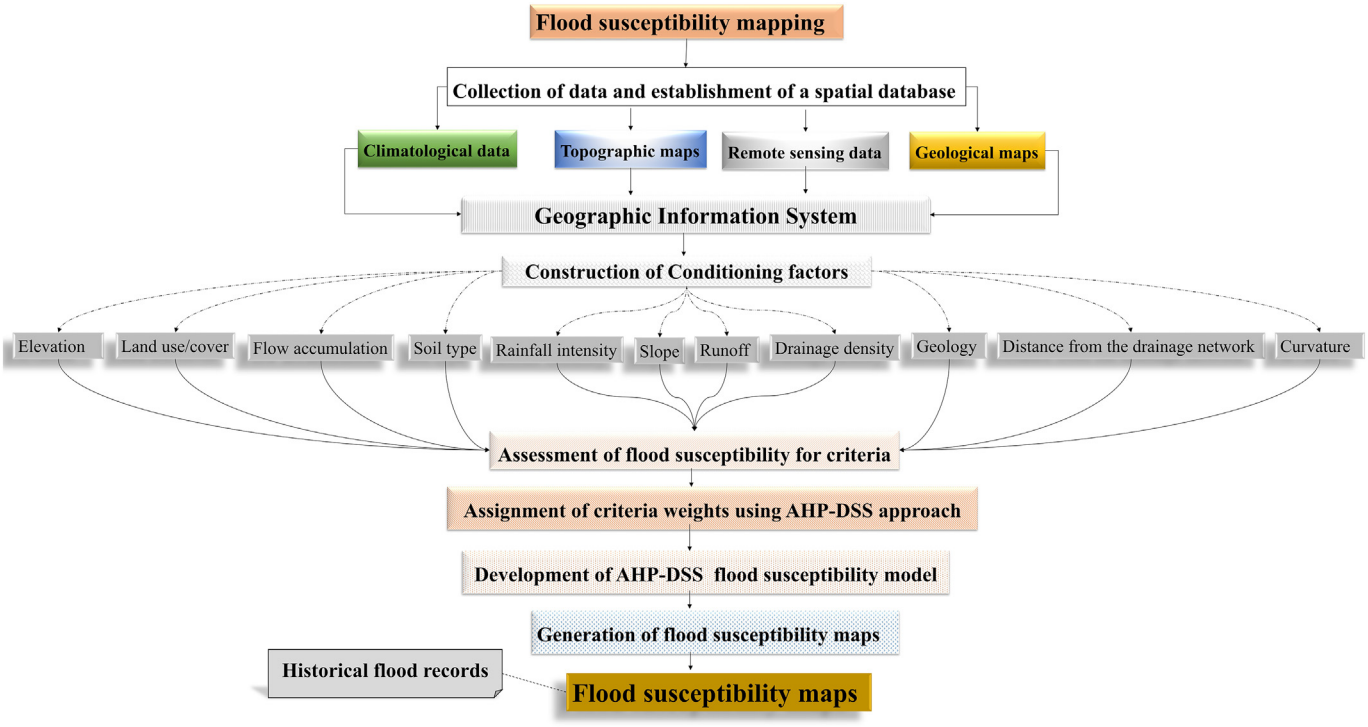

Fig. 2. Workflow chart.

The variance statistic is calculated as follow:

$$Var\,(S) = \frac{n(n-1)(2n+5) - \sum_{j=1}^{p} t_j(t_j-1)(2t_j+5)}{18} \tag{8}$$

where p is the number of groups in which each group consists of data points of equal values, and t_j is the number of data points in the jth group. Using the following Z-transformation, the statistic S is approximately normally distributed:

$$Z = \begin{cases} \dfrac{S-1}{(Var\,(S))^{0.5}} & if\ S>0 \\ 0 & if\ S=0 \\ \dfrac{S+1}{(Var\,(S))^{0.5}} & if\ S<0 \end{cases} \tag{9}$$

The slope (T_j) is computed according to Sen (1968) as follow:

$$T_j = \frac{x_j - x_i}{j-1} \tag{10}$$

The sign of the slope indicates if the trend of the time series is positive or negative.

3.2. Effects of urbanization in surface runoff

In general, there is a lack of surface runoff data in Egypt and Middle East Countries. Therefore, surface runoff data was estimated from the popular curve number method to transform to surface runoff and soil infiltration loss (Zhan and Huang, 2004; Bo et al., 2011). In the absence of detailed watershed information, this method is practical for it only requires general information such as landuse, treatment or practice, soil hydrologic condition, hydrologic soil group, and antecedent moisture condition to determine the curve number (CN) needed to estimate the storage at saturation and then the surface runoff. A composite or a really weighted CN is often for a river basin with several sub-regions (Zhan and Huang, 2004). The curve number method was applied to the two governorates based on their respective hydrological soil groups, land use, and slope.

A series of Landsat images of 1972–2014 were obtained from the U.S. Department of the Interior U.S. Geological Survey and classified into land use maps to track changes in urbanization over the years. The urban areas remained more or less unchanged over 1948–1970, but starting in 1970, urban areas gradually increased. Based on the hydrological soil groups, land use maps of different years, we calculated the CN for the two governorates, and update them every four years. From applying monthly rainfall data of 1948–2014 to the CN calculated, we derived the monthly and annual surface runoff data between 1948 and 2014. Next, two nonparametric change point tests, SNHT and Buishand's were applied on monthly, annual surface runoff, and surface runoff anomaly to detect possible change points in the surface runoff. The trends of these surface runoff data were estimated using the Mann–Kendall trend test. The magnitude of change in the surface runoff was estimated using Sen's slope method. There is no historical runoff data exist for the two study areas. So, our results were validated against annual surface runoff data of 2006–2014 and were found to agree well with recorded annual surface runoff.

3.3. Flood susceptibility mapping

After investigating effects of rapid urbanization and climate change in surface runoff, we developed the following flood susceptibility maps by an approach shown in Fig. 2 for the flood risk management of the two governorates of Egypt.

3.3.1. Selection criteria and data processing

Compared with past flood susceptibility studies, we have used a field survey and historical flood records of Egypt to identify eleven factors based on their relations to flooding in Egypt, to map flood susceptibility zones of the two governorates: land use/cover, rainfall intensity, runoff, flow accumulation, drainage density, distance from the drainage network, elevation, slope, soil type, geology, and curvature.

Table 1
Susceptibility levels of various watershed and climatic factors in relation to flooding.

SL.NO.	Thematic layers	Classes	Rating
1	Flow accumulation (pixels)	0–850	1
		850–1250	2
		1250–3415	3
		3415–17,525	4
		17,525–10,885,000	5
2	Distance to drainage network (m)	<150	5
		150–350	4
		350–750	3
		750–1250	2
		>1250	1
3	Elevation (m)	−26–18′	5
		18–70	4
		70–121	3
		121–172	2
		172–221	1
4	LULC	Irrigated cropland	3
		Grassland	2
		Shrubland	4
		Sparse vegetation	3
		Built up areas	5
		Vegetation regularly flooded	4
		Bare soil	2
		Water bodies	5
5	Rainfall intensity units MFI	0–42	1
		42–75	2
		75–105	3
		105–150	4
		150–191	5
6	Slope (%)	0–2	5
		2–5.	4
		5–15.	3
		15–35	2
		35–90	1
7	Geology	Holocene	3
		Pleistocene	2
		Quaternary	3
		Sea	5
		Cenozoic	2
		Water	4
8	Runoff (mm/yr)	0–25	1
		25–50	2
		50–75	3
		75–150	4
		150–184	5
9	Soil type	Dunes or shifting sands	1
		Calcaric Fluvisols	2
		Calcaric Regosols	4
		Eutric Gleysols	4
		Inland water	4
		Calcisols and gypsisols	3
		Calcic Yermosols	4
		Gleyic Solonchaks	5
10	Drainage density (km/km^2)	0–0.37	1
		0.37–0.65	2
		0.65–1	3
		1–2.9	4
		2.9–5.3	5
11	Curvature	Concave	1
		Flat	1
		Convex	3

3.3.2. Assessment of factors susceptibility level

From the literature review, and the ranking method of Saaty (1980), we ranked the above eleven factors with respect to their respective level of susceptibility and relevance to flood hazards as shown in Table 1. The susceptibility to flood in the two governorates is strongly related to the level of urbanization since surface runoff increases with urbanization. In contrast, permeable soils or areas with forest covers and shrubland tend to have lower surface runoff (Jacinto et al., 2014). In other words, soil types affect the water holding capacity and infiltration characteristics of an area which consequently affects its susceptibility to flood (Nyarko, 2002). According to Hill et al. (2010), even under dry moisture conditions, flooding can occur in clayey soil subjected to intensive rainfall. Rainfall intensity also plays an important role in flood susceptibility, for more intensive rainfall events lead to more surface runoff and vice versa. A densed drainage network and steeper slope can also lead to significant increase in surface runoff, and so more likely to result in flooding, especially in areas located close to flow accumulation path. Each flood susceptibility factor in Table 1 is classified under five classes, ranging from very high to very low flood susceptibility as follows: 5 "very high flood susceptibility", 4 "high flood susceptibility", 3 "moderate flood susceptibility", 2 "low flood susceptibility" and 1 "very low flood susceptibility".

3.3.3. Assignment of weights to watershed and climatic factors

Under an analytical hierarchy process, watershed and climatic factors were assigned with weights using the pairwise ranking and rank sum methods. The TerrSet Geospatial Monitoring and Modeling System was used to obtain optimal weights from the principal eigenvector of the pairwise comparison matrix (Janssen and Herwijnen, 1994). The rank sum method of Eq. (11) was used to validate weights derived for each flood related factor based on the pairwise comparison between each two factors.

$$W_k^{\mathrm{rs}} = \frac{n+1-k}{\sum_{i=1}^{n}(n+1-i)} \tag{11}$$

where W is the weighting factor while k of number 1 to 11 represents one of the flood related factors. The accuracy of each pairwise comparison was assessed by the consistency index of Saaty (1977, 1980, 1990), which is a measure of departure from the consistency or inconsistency of pairwise judgments in the comparison matrices. The analytical hierarchy process for rating each cell in the matrix is shown in Table 2. This rating was systematically calculated in a pairwise comparison approach via a matrix operation by multiplying factors of a row with other factors of a corresponding column. Because the matrix is symmetrical, it is only necessary to compute the ratings for half of the matrix.

The consistency ratio of the matrix obtained was 0.06 which means an acceptable consistency (Saaty, 1977). The final consistency ratios obtained for each flood related factor are shown in Table 3.

4. Results and discussions

4.1. Impact of climate change in flood risk

From applying SNHT and Buishand's change point detection techniques to temperature anomalies between 1948 and 2014, a statistically significant change point in temperature anomaly was detected in 1976 (Fig. 3), because the mean temperature anomaly of −0.333 °C/yr between 1948 and 1976 increased to 0.242 °C/yr between 1976 and 2014. This increase in temperature anomaly is attributed to climate change caused by rising concentration of greenhouse gases, rapid urbanization, and deforestation (Grimmond, 2007; Ren et al., 2008; Yan et al., 2010; Banasik et al., 2014). A statistically significant warming trend of 0.16 °C/decade in the two governorates was detected by the Mann–Kendall trend test (Table 4). Similar studies show that urbanization or more impervious surfaces have led to rising temperature in urban areas and higher surface runoff than in non-urban areas of the same governorates (Bounoua et al., 2015).

To investigate if climate change impact has contributed to recent flooding in the two governorates, we conducted trend analysis and change point detection in annual rainfall and rainfall anomalies. Both SNHT and Buishand's tests detected statistically significant change points in annual rainfall and rainfall anomalies in 1994, because the average annual rainfall decreased from 139.73 mm/yr between 1948 and 1994 to 98.82 mm/yr between 1994 and 2014 (Fig. 4). Trend analysis also reveals statistically significant declining trends in annual rainfall since 1994 at the rate of 8.96 mm/decade. To further confirm the declining trend in annual rainfall we checked rainfall anomalies. Similarly,

Table 2
Factors of flood susceptibility: analytical hierarchy process.

Factors	Flow accumulation	Distance	Elevation	Land use/cover	Rainfall intensity	Slope	Geology	Runoff	Soil type	Drainage density	Curvature
Flow accumulation	1	2	2	3	3	5	7	1	2	2	7
Distance drainage network	1/2	1	1	2	2	3	4	1/2	1/4	1	4
Elevation	1/2	1	1	2	2	2	5	1/3	1/2	1	5
Land use/cover	1/3	1/2	1/2	1	2	5	5	1/2	1/5	1/2	3
Rainfall intensity	1/3	1/2	1/2	1/2	1	3	4	1/2	1/2	1/3	4
Slope	1/5	1/3	1/2	1/5	1/3	1	3	1/4	1/2	2	3
Geology	1/7	1/4	1/5	1/5	1/4	1/3	1	1/6	1/3	1/3	2
Runoff	1	2	3	4	2	4	6	1	2	4	6
Soil type	1/2	4	2	5	2	2	3	1/2	1	2	3
Drainage density	1/2	1	1	2	3	1/2	3	1/4	1/2	1	3
Curvature	1/7	1/4	1/5	1/3	1/5	1/3	1/2	1/6	1/3	1/3	1

statistically significant declining trends were detected in rainfall anomaly at 15.3 mm/decade (Fig. 5).

Under a warming trend since 1976 of 0.16 °C/decade, it seems that climate change has resulted in a significant decline in rainfall anomalies and annual rainfall in the two governorates. According to some past studies, urbanization has a major effect on the surface energy budget of the atmosphere (Kerschgens and Drauschke, 1986), resulted in the heat island effect in addition to climate warming caused by greenhouse effects (Changnon and Huff, 1986). Cao et al. (2018) studied the impact of rapid urbanization on the summer temperature in eastern China where they projected extensive warming trends up to 5 °C, 3 °C, and 2 °C under three different urban growth scenarios. According to Arsiso et al. (2018), land use change is the second most important anthropogenic influence on climate beside the emission of greenhouse gases, e.g., they reported that urbanization has caused climate warming. In addition, urbanization has also contributed to increased flood risk in many regions globally (Gu et al., 2011; Birhanu et al., 2016). In China, Gu et al. (2011) reported an increase in flood susceptibility because of rapid urbanization. Similarly, Birhanu et al. (2016) found that rapid urbanization has resulted in an increase in flood susceptibility of Addis Ababa of Ethiopia. Some studies even found a causal relationship between urbanization and carbon emissions. For example, Xu et al. (2018) reported that urbanization had the most obvious impact on carbon emissions of the Pearl River Delta of China; Fu and Weng (2016) found that urbanization has resulted in a significant increasing trend of about 1.8 °K per decade in the metropolitan area of Atlanta, Georgia, USA.

4.2. Effects of urbanization on surface runoff

The monthly surface runoff estimated by the CN method show high temporal variability between 1948 and 2014. Statistically significant change points were at 1984, after which monthly surface runoff increased from 2.47 mm/m between 1948 and 1984 to 7.23 mm/m between 1984 and 2014. Despite of a decline annual precipitation, a statistically significant positive trend in monthly surface runoff at 0.015 mm/m (18 mm/decade) was also detected after 1984 (Fig. 6) because of rapid urbanization, as reflected in higher curve number in the two governorates. Long-term monthly surface runoff ranges from 0 to 99 mm/month, with the highest surface runoff since 1984 occurring in January, February, November, and December, which have been the months with recurrent flooding every year, where 50 to 99 mm of surface runoff could be generated in a few hours. In the last few decades, because of noticeable increase in impervious surfaces in Alexandria and El-Beheira, more surface runoff has been generated, which shows the effects of urbanization on the flood risk of arid regions of Egypt.

Because of urbanization, annual surface runoff in the two governorates has been relatively high with respect to the annual precipitation. Annual surface runoff range widely, from 2.29 mm/yr to 242.86 mm/yr, with a long-term annual mean of 57.5 mm/yr and a standard deviation of 53.2 mm/yr. According to the surface runoff data estimated using the CN method, the two governorates generated >150 mm/yr of surface runoff in 1991, 1992, 1994, 2000, 2002, 2006, 2009, 2012 and 2013. The last four years of high surface runoff estimated agree with historical flooding records of the two governorates in 2006, 2009, 2012 and 2013. The effects of urbanization in surface runoff become clearer by increasing the time scale of the analysis (Fig. 7). Other studies also found that rapid urbanization has led to increased surface runoff (Guan et al., 2016; Chen et al., 2017; Bian et al., 2017). From the statistically significant change point in surface runoff detected in 1970, the mean annual surface runoff had increased from 21.15 mm/yr between 1948 and 1970 to 76.55 mm/yr between 1970 and 2014. In other words, the annual runoff had been increasing at a statistically significant positive trend of 12.7 mm/decade since 1970s, which agrees with rapid urban expansion after 1970. This was partly because between 1970 and 2014, Egypt had experienced a significant increase in population from 35 million in 1970 to >100 million in 2014.

Similarly, the analysis of surface runoff anomalies (Fig. 8) shows significant temporal variations with a change point detected in 1970, such that the mean surface runoff anomaly increased from −36.38 mm/yr between 1948 and 1970 to 19.02 mm/yr between 1970 and 2014. This means a statistically significant positive trend of 14.39 mm/decade after 1970. Again, years with relatively high surface runoff anomalies

Table 3
Normalized flood susceptibility factors: analytical hierarchy process.

	Flow accumulation	Distance	Elevation	Land use/cover	Rainfall intensity	Slope	Geology	Runoff	Soil type	Drainage density	Curvature
Flow accumulation	0.19	0.16	0.17	0.15	0.17	0.19	0.17	0.20	0.25	0.14	0.17
Distance drainage network	0.10	0.08	0.08	0.10	0.11	0.11	0.10	0.10	0.03	0.07	0.10
Elevation	0.10	0.08	0.08	0.10	0.11	0.08	0.12	0.07	0.06	0.07	0.12
Land use/cover	0.06	0.04	0.04	0.05	0.11	0.19	0.12	0.05	0.02	0.03	0.07
Rainfall intensity	0.06	0.04	0.04	0.02	0.06	0.11	0.10	0.10	0.06	0.02	0.10
Slope	0.04	0.03	0.04	0.01	0.02	0.04	0.07	0.05	0.06	0.14	0.07
Geology	0.03	0.02	0.02	0.01	0.01	0.01	0.02	0.03	0.04	0.02	0.05
Runoff	0.19	0.16	0.25	0.20	0.11	0.15	0.15	0.20	0.25	0.28	0.15
Soil type	0.10	0.31	0.17	0.25	0.11	0.08	0.07	0.10	0.12	0.14	0.07
Drainage density	0.10	0.08	0.08	0.10	0.17	0.02	0.07	0.05	0.06	0.07	0.07
Curvature	0.03	0.02	0.02	0.02	0.01	0.01	0.01	0.03	0.04	0.02	0.02

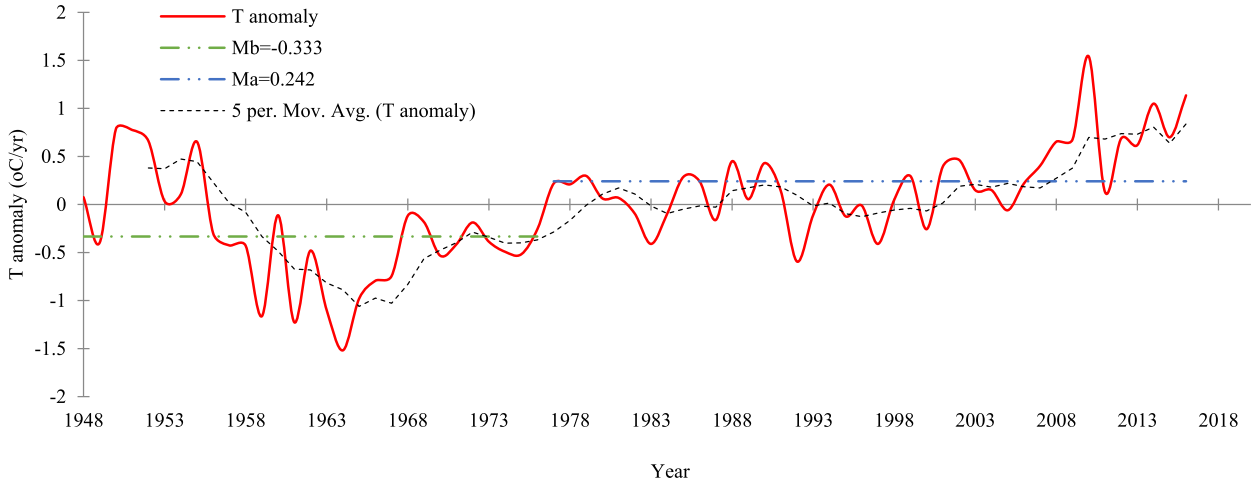

Fig. 3. Warming trend in temperature anomaly in the two governorates.

are 1991, 1992, 1994, 2000, 2002, 2003, 2006, 2009, 2012 and 2013 since surface runoff increased with rapid urbanization. The estimated surface runoff anomalies also agree with historical flood records in 2006, 2009, 2012 and 2013 in both governorates, respectively. Similarly, surface runoff anomalies with reference to the long-term, mean annual surface runoff has an increasing trend at 14.39 mm/decade. It seems that the curve number (CN) method applied to the two governorates has realistically accounted for the effects of urbanization on the surface runoff values.

After investigated the effect of climate change and urbanization on the surface runoff, we further developed the flood susceptibility model of the two governorates to identify their flood-prone areas useful for flood risk management.

4.3. Development of database for factors related to floods

4.3.1. Elevation, slope and flow accumulation

Digital elevation model (DEM) and its derivatives are very useful to develop flood susceptibility model in any region (Pradhan, 2009). DEM data of 30 m resolution (Fig. 9a) was obtained from the U.S. Department of the Interior U.S. Geological Survey to generate a map representing the slope (%) of the study area (Fig. 9b). As expected, flood prone areas are detected in low lying and flat areas. In relating elevation/slope to flood susceptibility, the two governorates were divided into five elevations and five slope zones. On the basis of historical flood records, low lying areas (elevations between −26 and +18 m) with mild slopes (0 to 2%) are prone to flooding and so are assigned with very high flood ratings, and vice versa. In contrast, steep slopes tend to have rapid flows and so are less prone to flooding. Next, areas with 2–5% slope are also relatively susceptible to flooding, areas with 5–15% slope are moderately susceptible to flooding, while areas with 15–35% slope or higher have low to very low susceptibility to flooding. Fig. 9c shows accumulation paths that contribute flow to a specific cell (group of pixels). Flow paths or drainage networks in a flow accumulation map identify cells where water will potentially accumulate, or where surface runoff will converge. Therefore, flow accumulation is crucial in flood studies for an increase in the accumulation of flow to an area or cell means an increase in the flood susceptibility of that area/cell (Lehner et al., 2006).

In an area represented by a set of pixels joined together spatially, the numbers of surrounding pixels that contribute flow to a particular pixel vary widely, ranging from small to very high numbers. In general, pixels that represent buildings or municipal infrastructure tend to have a larger number of pixels that contribute to flow. In Fig. 9c, red and blue-green pixels are those with high flow accumulation, green and yellow pixels have lower, while grey pixels have very low flow accumulation. Pixels with high flow accumulation are where surface runoff tends to converge (concentrated flow) and consequently are vulnerable to flood hazards, and vice versa. In this study, the total number of pixels in the flow accumulation map is 10,885,000. These pixels are divided into five zones, pixels with very low (0–850) to very large (17525–10,885,000) number of pixels contributing to flow accumulation.

4.3.2. Drainage density and distance to drainage network

The drainage density maps of the two governorates, defined as the total length of all streams in a drainage basin divided by the total area of the drainage basin, (Fig. 9d) was prepared using the density analysis tool of ArcGIS. In these maps, the drainage density is classified into five classes, such that a dense drainage network means a high flow accumulation path and more likely to get flooded. These five classes are categorized as 'very high' (2.9–5.3 km/km^2), 'high' (1–2.9 km/km^2), 'moderate' (0.65–1 km/km^2), 'low' (0.37–0.65 km/km^2), and 'very low' (0–0.37 km/km^2) drainage density, respectively. Furthermore, areas located close to the drainage network and flow accumulation path tend to have a higher susceptibility to flooding (Islam and Sado, 2000). To delineate flood susceptible zones based on the proximity to

Table 4
Climate variables and surface runoff change detection and trend.

		SNHT				Buishand's test						Mann-Kendall trend test			
Variable	Year	T0	T	p-Value	Trend	Q	T	p-Value	Trend	Mb	Ma	Kendall's tau	p-Value	Trend	Sen's slope
Annual rainfall	1948–2014	4.39	1994	0.03875	Ha	7.9072	1994	0.0232	Ha	139.7	98.82	0.18	0.0009	−	0.896
Rainfall anomaly	1948–2014	4.39	1994	0.0393	Ha	7.9072	1994	0.0236	Ha	12.21	−28.7	0.316667	0.0089	−	1.530
Temperature anomaly	1948–2014	20.781	1976	<0.0001	Ha	17.802	1976	<0.0001	Ha	−0.333	0.242	0.371349	<0.0001	+	0.016
Monthly runoff	1948–2014	34.641	1984	0.0141	Ha	83.081	1984	<0.0001	Ha	2.47	7.23	0.089591	0.0003	+	0.015
Annual runoff	1948–2014	21.814	1970	0.0021	Ha	18.469	1970	<0.0001	Ha	21.15	76.55	0.533333	<0.0001	+	1.27
Runoff anomaly	1948–2014	21.814	1970	0.0015	Ha	18.469	1970	<0.0001	Ha	−36.38	19.02	0.533333	<0.0002	+	1.439

Ha: There is a trend in the series, Negative sign: downward trend, Positive sign: upward trend, T: year of the change point, Mb-mean value before change point, Ma mean value after change point.

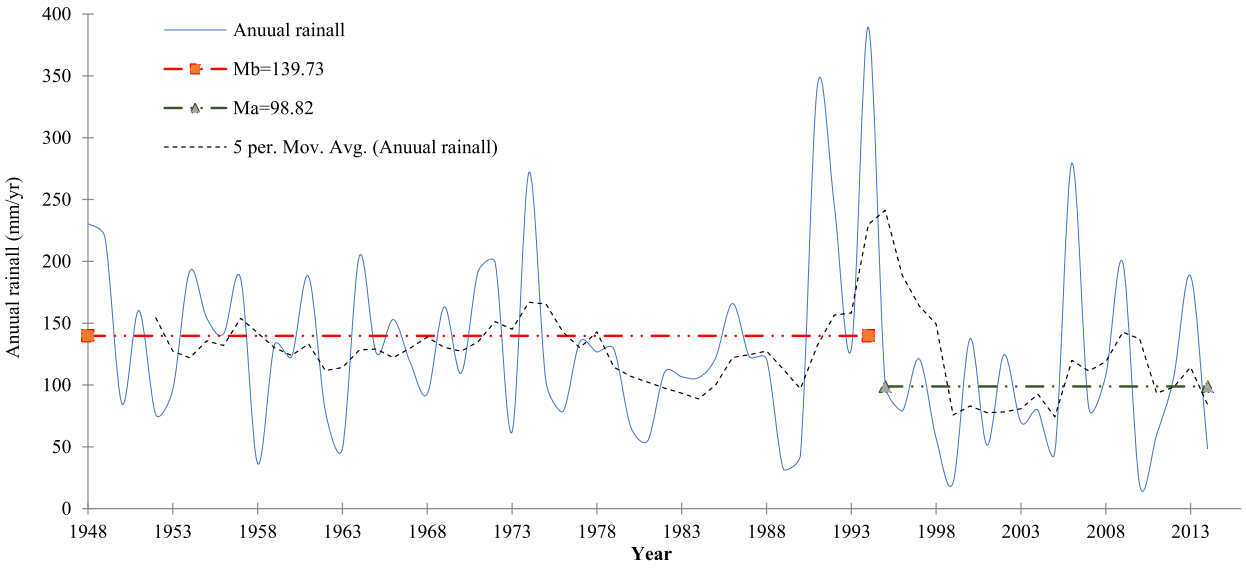

Fig. 4. Mean annual rainfall time series and trend in the two governorates.

the flow path defined as the buffer distance, the two governorates were delineated into five classes with very high, high, moderate, low and very low susceptibility to flooding (Fig. 9e), which are validated against records of areas subjected to historical floods. Based on the historical flood record, areas located within 150 m from the drainage network were classified as areas highly susceptible to flood hazard. Next, areas that are at a distance of 350, 750, 1250 and >1250 m from the drainage network are classified as areas of high, moderate, low and very low, susceptibility to flooding hazards, respectively. As expected, areas near the drainage network (within 150 m) are highly susceptible to flood hazard, which decreases as the distance away from the river network increases, as found in other studies, e.g., Kazakis et al. (2015).

4.3.3. Land use/cover, rainfall intensity and surface runoff

To track how urbanization has contributed to increase in the surface runoff of Egypt, we also categorized a Landsat image every four years between 1970 and 2014 into classes of landuse for the two governorates by supervised classification, e.g., training samples of various land use types were collected in field surveys and matched with spectral signatures of corresponding pixels of Landsat images (Fig. 9f shows the land use map of 2014). Landsat images are remotely sensed data widely used to monitor the environment, e.g., Hossain et al. (2013), Biftu and Gan (2004). Eight landuse classes were identified: irrigated cropland, grassland, shrubland, sparse vegetation, built-up areas, vegetation regularly flooded, bare soil and water bodies. The classified images were validated using the Kappa Agreement Index (KIA) where a KIA value exceeding 0.8 represents good classification performance (Jensen, 2005). The overall KIA statistic obtained was 0.938 which demonstrates that the classified land use maps are accurate. Under moderate storms, our analysis shows that flooding is more likely to occur in an urban than a rural environment.

Rainfall intensity (Fig. 9h) is expressed by a modified Fournier index (MFI) which is the sum of mean monthly rainfall intensity estimated from 66 years of monthly rainfall data. As high surface runoff corresponds to months and years of the high rainfall intensity, high rainfall intensity means more susceptibility to flash flooding and vice versa. Despite of low annual rainfall, a major cause of flooding in the study area are infrequent occurrences of extremely heavy, short-duration rain storms over soils of low water absorptive capacity, resulting in excessive overland flow which, enhanced by urbanized land of steep relief converges to the channel network as a flash flood. Therefore, despite generally low annual rainfall in Egypt, the occurrences of very intensive storms still result in flooding problems. For the study area, MFI values that range between 28 and 191 mm/yr are classified into five classes according to the potential for flood occurrences (Table 1). From the 1948–2014 surface runoff data for the two governorates, surface runoff

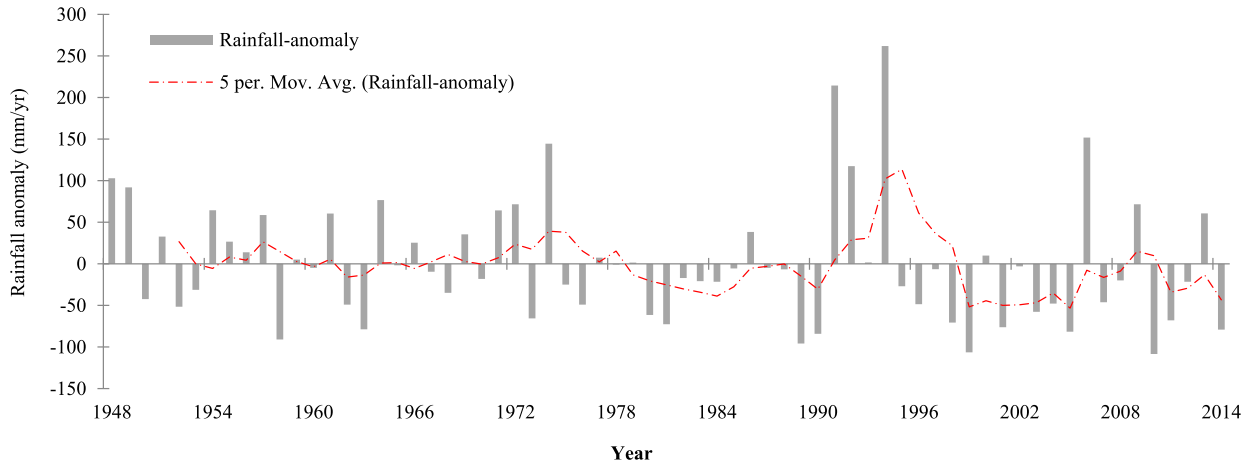

Fig. 5. Rainfall anomaly in the two governorates.

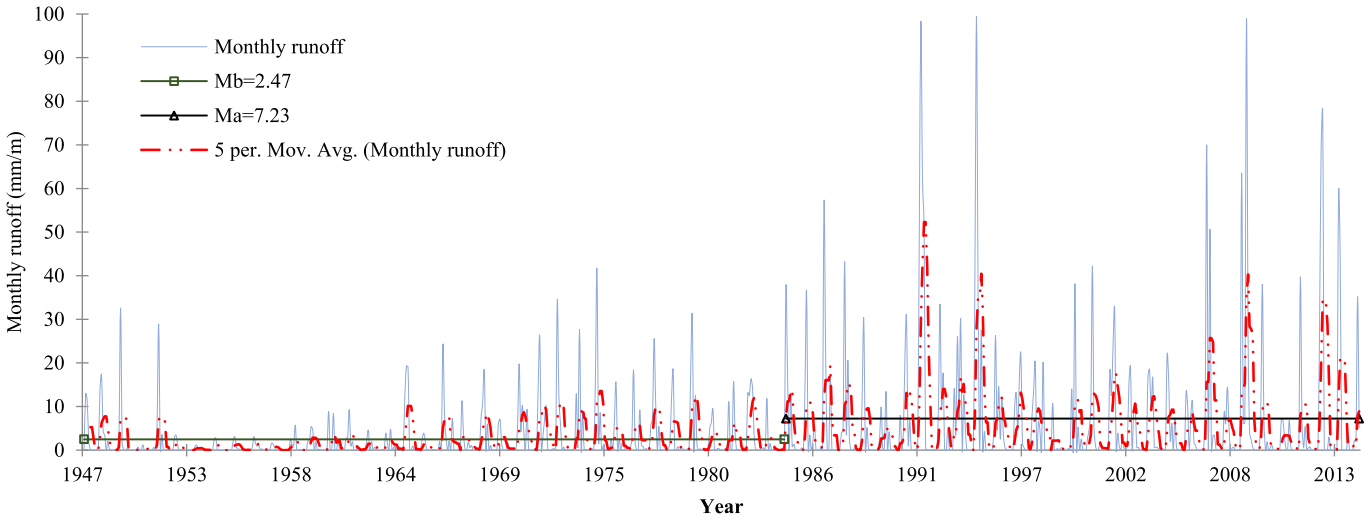

Fig. 6. Urbanization implication in monthly surface runoff time series, and trend in the two governorates.

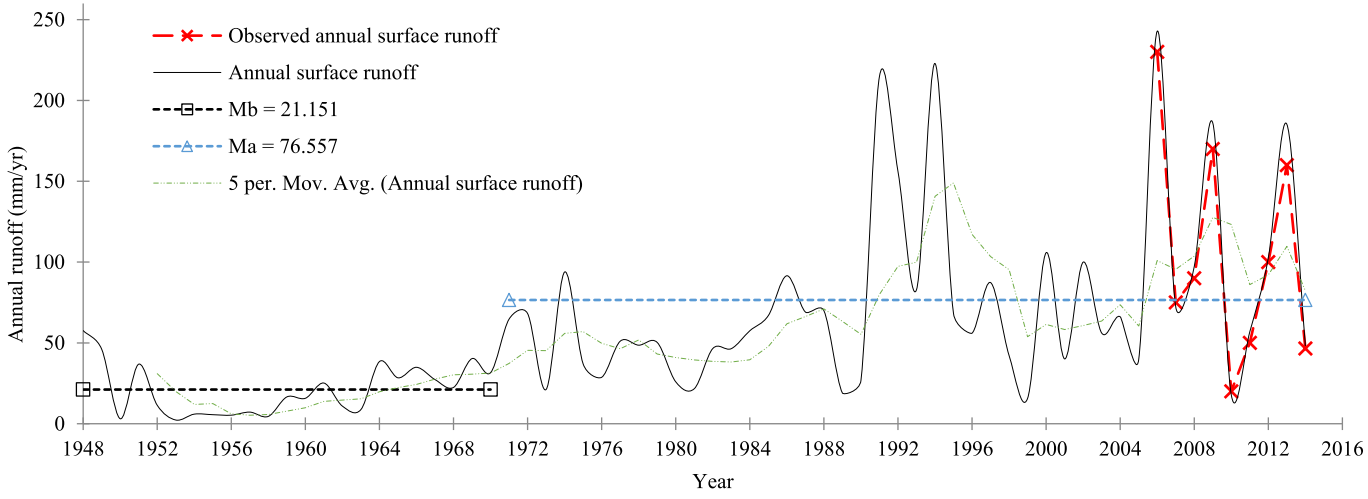

Fig. 7. Annual surface runoff time series, and trend in the two governorates.

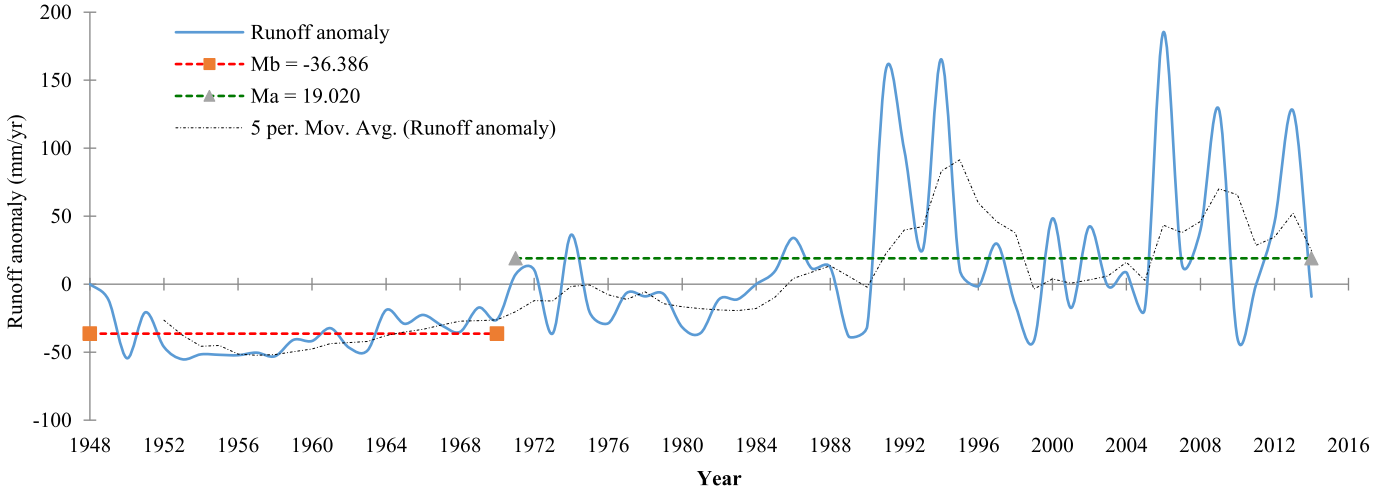

Fig. 8. Surface runoff anomaly time series, and trend in the two governorates.

varies from as low as 4 to a max of 184 mm/year (see the latest surface runoff of Fig. 9i). The runoff depth tends to increase in urban areas due to compacted soils and the presence of impervious areas because of urbanization, which leads to periodic occurrences of flash floods in Alexandria and Beheira.

The highest runoff depth was recorded within northern and northeastern parts of the Beheira governorates, which contain following regions: Edko, El Mahmoudiyah, Abu Hummus, Rosetta, Shubrakhit, Damanhur, Rahmaniya, Kafr el-Dawwar, and Wadi El Natrun, with surface runoff depth ranging from 65 to 184 mm/year. High runoff depths (81–184 mm/yr) have also occurred in northeastern and northwestern parts of Alexandra that consists of following cities: Montazah, El-Raml, Sidi Gaber, Bab Sharq, Al Attareen, Moharrem Beik, El-Dekheila, El-Agamy, and El-Ameriah. Towards south and western parts of Alexandria (Karamouz and Mina El-Bassal) and southwestern region of Beheira, the runoff depth tends to be slightly lower because these regions are dominated by agriculture land. However, these areas recently suffered unexpected flash floods which incurred huge damages. Given major historical floods had occurred for surface runoff higher than 150 mm/yr, e.g., the likelihood of a flood risk increases as the amount of surface runoff increase, the runoff depth map was classified as follows: 'very high susceptibility' (150–184 mm/yr), 'high susceptibility' (75–150 mm/yr), 'moderate susceptibility' (50–75 mm/yr), 'low susceptibility' (25–50 mm/yr), and 'very low susceptibility' (0–25), respectively.

4.3.4. Soil type, geology and curvature

The soil map of the two governorates was prepared from the soil data published by the Egyptian government (Fig. 9j), with following main soil types identified according to the FAO (1974) soil classification procedure: Calcaric Fluvisols; Calcaric Regosols; Calcic Yermosols; Gleyic Solonchaks; Eutric Gleysols; Calcisols; Gypsisols and shifting

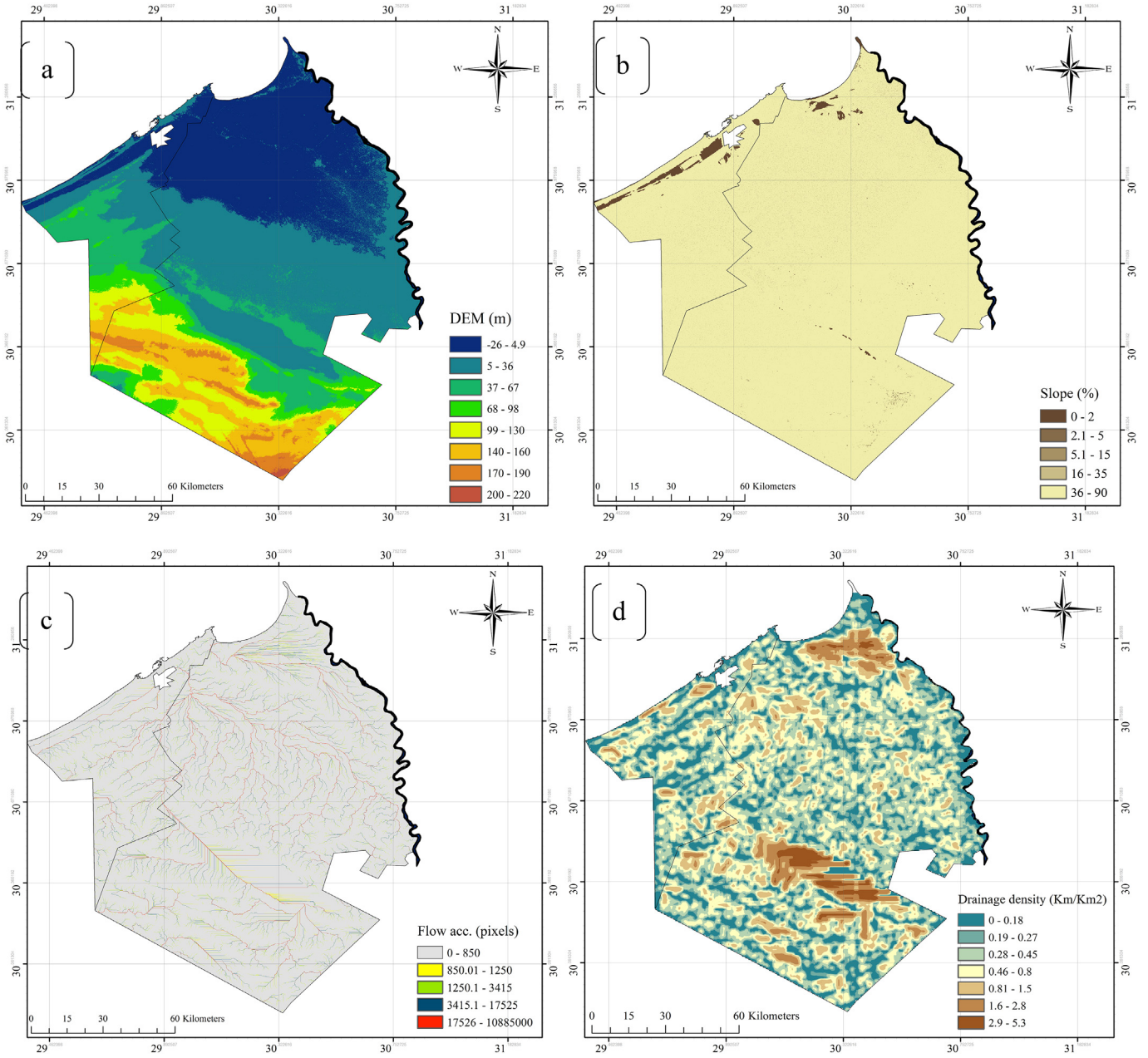

Fig. 9. Conditioning factors for flood susceptibility: (a) DEM, (b) slope, (c) flow accumulation, (d) drainage density, (e) distance from the drainage network, (f) land use/cover, (h) rainfall intensity, (i) runoff, (j) geology, (k) soil type, (l) curvature.

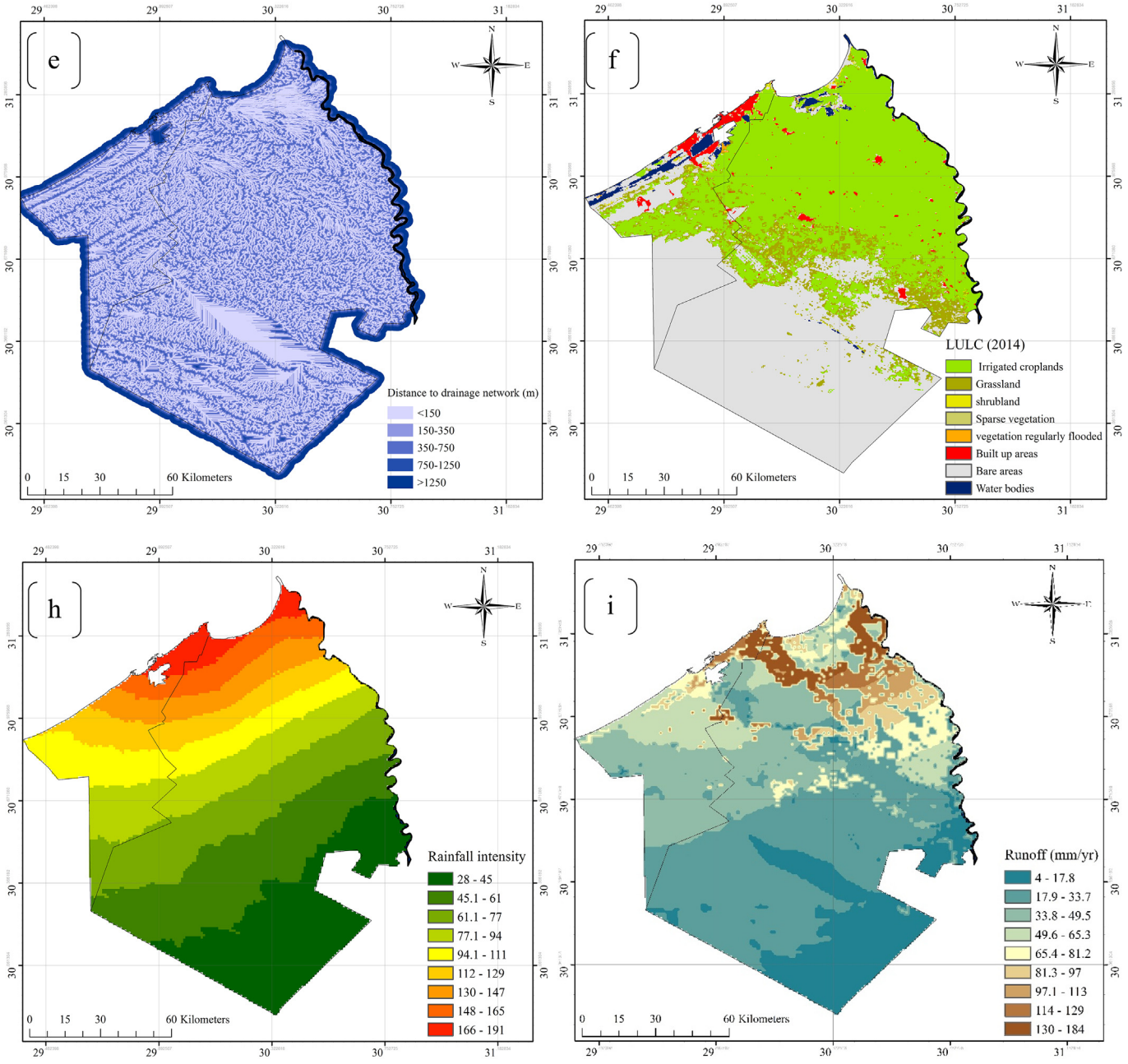

Fig. 9 (*continued*).

sands. Calcaric Fluvisols soils have the potential to become croplands because of their high infiltration rate which reduces the soil erosion problems and the susceptibility to flooding. Calcaric Regosols soil can be found in highly urbanized, coastal lowlands of Alexandria where flooding is usually a major concern. Calcic Yermosols soils consist of clay accumulation and therefore of high susceptibility to flooding. Gleyic Solonchaks and Yermosols soils have moderate to low infiltration rate due to high clay content. Eutric Gleysols soils also tend to be easily saturated, and so are highly susceptible to flooding. Calcisols and gypsisols soils have poor water-holding capacity, and of low susceptibility to flooding due to the low clay content.

Fig. 9k shows six geological groups in the two governorates assigned with various susceptibility levels to flooding: Holocene, Pleistocene, Quaternary, Cenozoic, and rocks undersea and rocks with groundwater. Cenozoic rocks and Pleistocene sand and gravel rocks (Itoh et al., 2001) are assigned low susceptibility to flood occurrences because of high hydraulic permeability; while both Quaternary rocks and Holocene clay deposits are assigned moderate susceptibility to flooding because of high porosity, and moderate to high permeability, respectively. We used ArcGIS 10.1 to produce the curvature map (Fig. 9l) of which a positive curvature is convex, a zero curvature is flat, and a negative curvature is concave, respectively. Curvature highly influences the surface flow, for concave and flat shapes tend to retain more water and for a longer period than convex shapes (Moghaddam et al., 2015; Lee and Pradhan, 2006). Therefore, concave/flat shapes are considered as low flood susceptibility zones while convex shapes as high flood susceptibility zones because a convex slope could generate higher surface runoff than a concave slope during heavy rainfall.

5. Flood susceptibility zones

Finally, after developing the flood susceptibility model, physical factors related to flooding, we used the model and the information to generate flood susceptibility maps by combining the eleven-factor maps

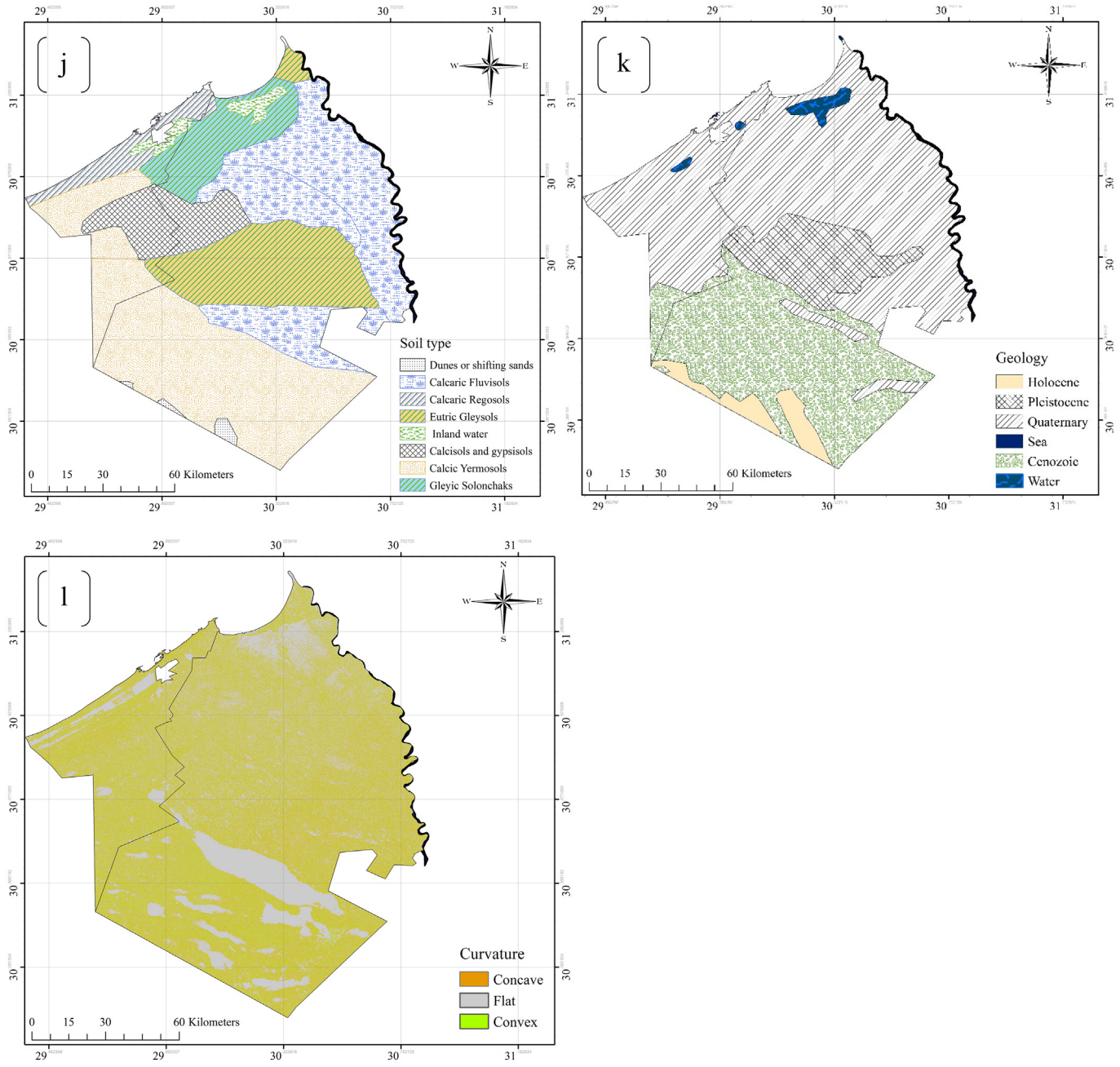

Fig. 9 (*continued*).

using a weighted approach from weighting factors developed in Table 5 and the weight module of TerrSet Geospatial Monitoring and Modeling System. The susceptibility model generated flood susceptibility maps for both governorates, each with five vulnerability classes ranging from Very high, High, Moderate, Low, to Very low. For the Beheira governorate area (Table 6), 9.2% (930.1 km^2) and 17.9% (1815.2 km^2), 32.3% (3269.7 km^2), 28.3% (2869.2 km^2) and 12.3% (1245.8 km^2) are assigned very high and high susceptibility, moderate, low and very low

Table 5
Weight (percent of influence).

SL.NO.	Thematic layers	Weight	Weight %
1	Flow accumulation	0.178	17.8
2	Distance drainage network	0.089	8.9
3	Elevation	0.090	9.0
4	Land use/cover	0.073	7.3
5	Rainfall intensity	0.066	6.6
6	Slope	0.052	5.2
7	Geology	0.025	2.5
8	Runoff	0.189	18.9
9	Soil type	0.138	13.8
10	Drainage density	0.079	7.9
11	Curvature	0.022	2.2

Table 6
Classes of flood susceptibility and number of historical flood events.

	Beheira governorate			Alexandria governorate		
Flood susceptibility	Area (km^2)	Area (%)	# of events	Area (km^2)	Area (%)	# of events
Very low	1245.8	12.3	–	19.7	0.8	–
Low	2869.2	28.3	1	220.6	8.8	–
Medium	3269.7	32.3	4	1028.3	41	1
High	1815.2	17.9	17	841.9	33.5	9
Very high	930.1	9.2	21	400.1	15.9	14

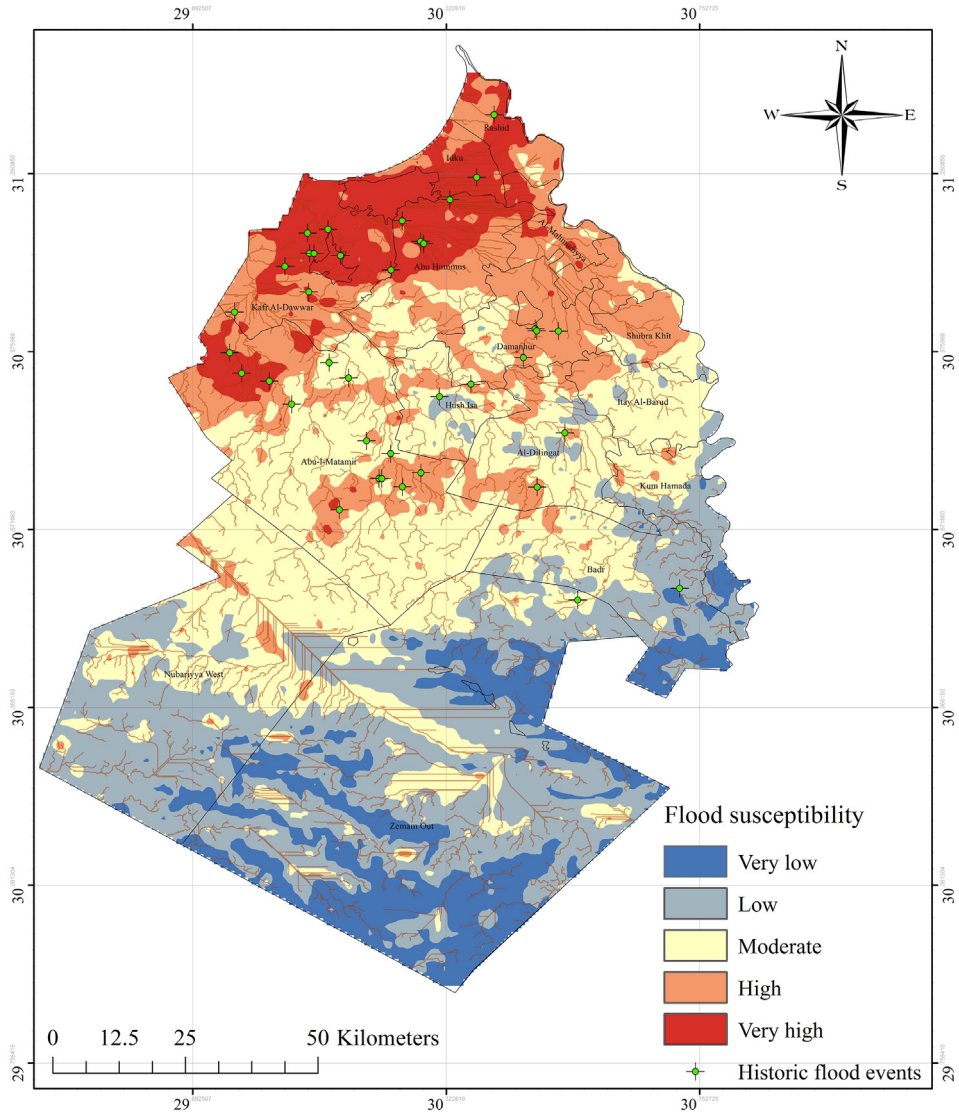

Fig. 10. Flood susceptibility map for the districts of Beheira governorates.

susceptibility, respectively. For the Alexandria governorate area, 15.9% (400.1 km^2), 33.5% (841.9 km^2), 41% (1028.3 km^2), 8.8% (220.6 km^2) and 0.8% (19.7 km^2) are assigned very high and high susceptibility, moderate, low and very low susceptibility, respectively (Table 6).

Fig. 10 shows the spatial distribution of flood susceptibility zones in Beheira governorate where most of very high and high susceptible zones are located in northern, northwestern and northeastern parts, which consist of the following areas: Edko, El Mahmoudiyah, Aboul Matamir, Abu Hummus, Rosetta, Shubrakhit, Damanhur, Rahmaniya, Kafr el-Dawwar, and Wadi El Natrun. In the last few decades, there had been an increasing trend in the occurrence of flood events due to rapid urbanization. Flooding in these areas has been occurring every winter, causing heavy damage to roads, agricultural lands, and cities. In November 2015, the low-lying areas in Wadi al-Natrun, al-Rahmaniya, Aboul Matamir, Kafr al-Dawar and Edko areas were flooded by heavy rainfall event, as was also confirmed from the surface runoff estimated for El-Beheira. By a collaboration between Egyptian armed forces and Beheira local authorities, many lives were rescued from flooded homes during flood events. However, still twenty-five people were killed in the Beheira governorate, either from drowning or electrocution caused by heavy rain occurring in villages such as Wadi Al-Natroun Valley, El Mahmoudiyah, Abu Hummus, Rosetta, Shubrakhit, Damanhur, Rahmaniya, and Kafr el-Dawwar. Hundreds of schools were shut down due to floods. Large swathes of homeland in the region had been devastated as well.

The level of damage to areas affected by the flooding in Beheira governorate, which included cities such as Damanhour, Edkou, and Kafr El Dawar and in the Mediterranean city of Alexandria, had caused public outrage and provoked criticism of the government's negligence and cities' poor infrastructure. Therefore, the Egyptian government allocated two billion Egyptian pounds to help solving problems of flooding, such as upgrading the sewage and drainage systems of the coastal city of Alexandria and Beheira governorate, under the supervision of the military. There are also zones with high to moderate susceptibility to floods in El Delengat, Etay El Barud, Hosh Issa, Kom Hamada, Nubariyah, and Badr (see Fig. 10).

A good match between records of historical flood events and the developed flood susceptibility map for districts of Alexandria governorates (Fig. 11, Table 6) demonstrate the accuracy and credibility of the map since many recorded flood events fall within areas with high flood susceptibility, such as Montazah, El-Raml, Sidi Gaber, Bab Sharq, Al Attareen, Moharrem Beik, El-Dekheila, El-Agamy, and Borg El Arab. For example, in November 2015, Alexandria was paralyzed when a severe rainstorm amounted to five times the mean November rainfall occurred over the city within a few days, which left many streets flooded, slowed down the traffic, and the Burj Al Arab Stadium was inundated with flood

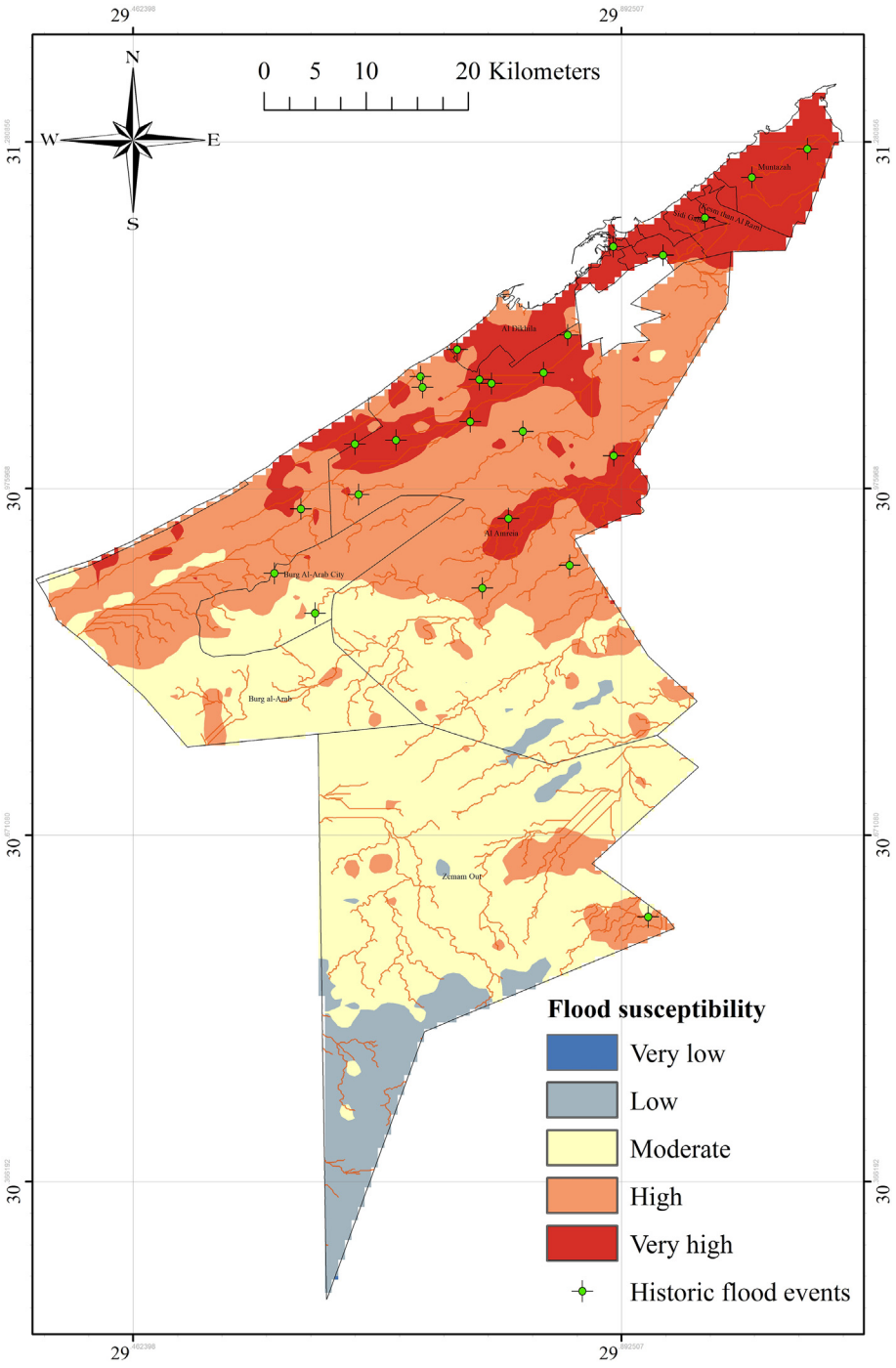

Fig. 11. Flood susceptibility map for Districts of Alexandria governorates.

water partly due to a lack of proper drainage systems. Seven people died from electric shock when a power cable of the tram line in Moharrem Beik fell into the flood water.

Furthermore, rising sea levels attributed to melting of Arctic sea ice, Greenland and glaciers worldwide because of climate change would also contribute to flooding in Alexandria, for seawater had flooded streets of Alexandria on multiple occasions. Despite a decrease in annual precipitation, unpredictable intesive rain events of short durations exacerbate chances of flooding, compounded by poor drainage systems and rapid urbanization. Alexander the Great constructed the ancient Alexandria city on shores of the Mediterranean Sea in 332 BCE A part of that ancient city lies 6 to 8 m under seawater because of sea level rise in modern times (La La Riche, 1996). The areas submerged in seawater and surrounding coastal regions of Alexandria are evidence of the impact of changing climate. Since 1989, >58 m of coastlines have vanished every year in Rasheed, also known as Rosetta. Flooding in these areas could displace entire communities in Alexandria and in the low-lying Nile Delta, where Winter storms have flooded Alexandria's streets with seawater annually.

Therefore, flood susceptibility maps will be useful to the Egyptian Civil Defence authority for conducting rescue operations during flash flood events; for municipal planners and engineers in choosing suitable locations to implement developments in the two governorates; for land use planning and flood mitigation in municipalities. For example, according to these maps, northern and northeastern parts of Beheira governorates, and northeastern and northwestern parts of Alexandra will

likely be inundated during flood events, partly because of their poor, under-developed drainage systems.

We considered eleven contributing factors in developing flood susceptibility maps, such as surface runoff, flow accumulation, soil type, rainfall intensity, drainage density, land use, slope, and others, which are generally more than factors considered in other studies. For instance, probably due to a lack of available information, Kazakis et al. (2015) who used seven flood contributing factors: flow accumulation, distance from the drainage network, elevation, land use, rainfall intensity and geology to map flood susceptibility zones in Rhodope–Evros region of Greece, considered flow accumulation as the most important contributing factor to flood, instead of surface runoff. In another study by Elkhrachy (2015), even though he also ranked surface runoff as the most important contributing factor, the weighting factor assigned for surface runoff of 35.5% may be too high (compared to 18.9% in our study) partly because he only used six factors in his study.

6. Conclusions and recommendations

In this study, we investigated the effects of urbanization and climate change to the flood risk of Beheira and Alexandria governorates of Egypt, developed a flood susceptibility model, and their flood susceptibility maps useful for rescue operations during flood hazards. We investigated changes to annual rainfall and temperature, and effects of urbanization to flood risk by using the runoff curve number method to estimate surface runoff time series for the two governorates over 1948–2014. Anomalies in surface runoff were computed to examine the effect of urbanization on the surface runoff time series generated. Finally, we developed a GIS decision support system to delineate flood susceptibility zones in the two governorates of Egypt. Likely related climate change impact, the annual rainfall of the two governorates had declined since 1994 at about 8.96 mm/decade, while rainfall anomalies had declined at about 15.3 mm/decade which is statistically significant. Since 1976, the climate has been warming at about 0.16 °C/decade partly due to effects of rising concentrations of greenhouse gases and partly due to rapid urbanization with a noticeable increase in impervious surfaces in Alexandria and El-Beheira in recent decades. Because of urbanization, the flood risk of both arid regions has increased, despite of a decline in the annual rainfall, for the annual surface runoff show a significant increasing trend of 12.7 mm/decade after 1970 because of rapid urbanization in both two governorates. With reference to the long-term annual surface runoff, the surface runoff anomalies of both governorates show upward trend of 14.39 mm/decade after 1970.

The flood susceptibility model delineated flood susceptibility zones in the Beheira governorate to 9.2% (930.1 km^2), 17.9% (1815.2 km^2), 32.3% (3269.7 km^2), 28.3% (2869.2 km^2) and 12.3% (1245.8 km^2) of its area as very high, high moderate, low and very low susceptibility to flooding, respectively. In contrast, for Alexandria governorate, the flood susceptibility model delineated 15.9% (400.1 km^2), 33.5% (841.9 km^2), 41% (1028.3 km^2), 8.8% (220.6 km^2) and 0.8% (19.7 km^2) of its area as very high, high, moderate, low and very low susceptibility to flooding, respectively. The very high and high susceptible zones were located in the northern, northwestern and northeastern parts of the Beheira governorates, which include Edko, El Mahmoudiyah, Aboul Matamir, Abu Hummus, Rosetta, Shubrakhit, Damanhur, Rahmaniya, Kafr el-Dawwar, and Wadi El Natrun, where for the past decade flooding had occurred every winter, causing heavy damages to roads, agricultural lands and cities. Floods had also occurred in some high to moderate susceptible zones such as El Delengat, Etay El Barud, Hosh Issa, Kom Hamada, Nubariyah, and Badr. For the Alexandria governorates, areas classified as high and very high susceptible zones are Montazah, El-Raml, Sidi Gaber, Bab Sharq, Al Attareen, Moharrem Beik, El-Dekheila, El-Agamy, Borg El Arab, and El-Ameriah areas where many flood events had occurred. From checking historical flood events against flood susceptibility zones of these maps, the results show that they are in good agreement, which demonstrates the accuracy of these maps.

Similar surface runoff data developed for Beheira and Alexandria governorates can be replicated for other governorates of Egypt. Such data and flood susceptibility maps developed will be beneficial to planners and governments for choosing suitable locations for future developments to minimize potential flood damages in Beheira and Alexandria governorates. To develop representative flood susceptibility maps, as many flood contributing factors as possible should be considered unless appropriate data are not available.

Acknowledgments

This work is part of the doctoral research of the first author at the Department of Civil and Environmental Engineering, University of Alberta, and was funded by a recruitment scholarship of the University of Alberta, Natural Sciences and Engineering Research Council of Canada, and Floodnet of Canada. The authors would like to thank both reviewers for their constructive comments which have improved the quality of the paper.

References

Arsiso, B.K., Tsidu, G.M., Stoffberg, G.H., Tadesse, T., 2018. Influence of urbanization-driven land use/cover change on climate: the case of Addis Ababa, Ethiopia. Phys. Chem. Earth A/B/C https://doi.org/10.1016/j.pce.2018.02.009 (in press).

Banasik, K., Krajewski, A., Sikorska, A., Hejduk, L., 2014. Curve number estimation for a small urban catchment from recorded rainfall-runoff events. Arch. Environ. Prot. 40 (3), 75–86.

Bian, G.D., Du, J.K., Song, M.M., Xu, Y.P., Xie, S.P., Zheng, W.L., Xu, C.Y., 2017. A procedure for quantifying runoff response to spatial and temporal changes of impervious surface in Qinhuai River basin of southeastern China. Catena 157, 268–278.

Biftu, G.F., Gan, T.Y., 2004. A semi-distributed, physics-based hydrologic model using remotely sensed and digital terrain elevation data for semi-arid catchments. Int. J. Remote Sens. 25 (20), 4351–4379.

Birhanu, D., Kim, H., Jang, C., Park, S., 2016. Flood risk and vulnerability of Addis Ababa City due to climate change and urbanization. Procedia Eng. 154, 696–702.

Bo, X.I.A.O., Qing-Hai, W.A.N.G., Jun, F.A.N., Feng-Peng, H.A.N., Quan-Hou, D.A.I., 2011. Application of the SCS-CN model to runoff estimation in a small watershed with high spatial heterogeneity. Pedosphere 21 (6), 738–749.

Bounoua, L., Zhang, P., Mostovoy, G., Thome, K., Masek, J., Imhoff, M., Shepherd, M., Quattrochi, D., Santanello, J., Silva, J., Wolfe, R., Toure, A.M., 2015. Impact of urbanization on US surface climate. Environ. Res. Lett. 10, 084010.

Buishand, T.A., 1982. Some methods for testing the homogeneity of rainfall records. J. Hydrol. 58 (1–2), 11–27.

Cao, Q., Yu, D., Georgescu, M., Wu, J., Wang, W., 2018. Impacts of future urban expansion on summer climate and heat-related human health in eastern China. Environ. Int. 112, 134–146.

Changnon, S.A., Huff, F.A., 1986. The urban-related nocturnal rainfall anomaly at St. Louis. J. Clim. Appl. Meteorol. 25, 1985–1995.

Chen, Y., Liu, R., Barrett, D., Gao, L., Zhou, M., Renzullo, L., Emelyanova, I., 2015. A spatial assessment framework for evaluating flood risk under extreme climates. Sci. Total Environ. 538, 512–523.

Chen, J., Theller, L., Gitau, M.W., Engel, B.A., Harbor, J.M., 2017. Urbanization impacts on surface runoff of the contiguous United States. J. Environ. Manag. 187, 470–481.

Cherqui, F., Belmeziti, A., Granger, D., Sourdril, A., Le Gauffre, P., 2015. Assessing urban potential flooding risk and identifying effective risk-reduction measures. Sci. Total Environ. 514, 418–425.

Elkhrachy, I., 2015. Flash flood hazard mapping using satellite images and GIS tools: a case study of Najran City, Kingdom of Saudi Arabia (KSA). Egypt. J. Remote Sens. Space. Sci. 18 (2), 261–278.

FAO, 1974. FAO-UNESCO Soil Map of the World, 1:5.000.000. UNESCO, Paris.

Fernández, D.S., Lutz, M.A., 2010. Urban flood hazard zoning in Tucumán Province, Argentina, using GIS and multicriteria decision analysis. Eng. Geol. 111 (1), 90–98.

Fu, P., Weng, Q., 2016. A time series analysis of urbanization induced land use and land cover change and its impact on land surface temperature with Landsat imagery. Remote Sens. Environ. 175, 205–214.

Gizaw, M., Gan, T.Y., 2015. Possible impact of climate change on future extreme precipitation of the Oldman, Bow and Red Deer River Basins of Alberta. Int. J. Climatol. https://doi.org/10.1002/joc.4338.

Grimmond, S.U.E., 2007. Urbanization and global environmental change: local effects of urban warming. Geogr. J. 173 (1), 83–88.

Gu, C., Hu, L., Zhang, X., Wang, X., Guo, J., 2011. Climate change and urbanization in the Yangtze River Delta. Habitat Int. 35 (4), 544–552.

Guan, M., Sillanpää, N., Koivusalo, H., 2016. Storm runoff response to rainfall pattern, magnitude and urbanization in a developing urban catchment. Hydrol. Process. 30 (4), 543–557.

Guha-Sapir, D., Below, R., Hoyois, P., 2014. EM-DAT: International disaster database. Univ. Cathol. Louvain, Brussels, Belgium www.em-dat.net, Accessed date: October 2018.

Hill, C., Verjee, F., Barrett, C., 2010. Flash Flood Early Warning System Reference Guide. University Corporation for Atmospheric Research (ISBN, 978-0).

Hong, H., Panahi, M., Shirzadi, A., Ma, T., Liu, J., Zhu, A.X., Chen, W., Kougias, I., Kazakis, N., 2017. Flood susceptibility assessment in Hengfeng area coupling adaptive neuro-fuzzy inference system with genetic algorithm and differential evolution. Sci. Total Environ. 621, 1124–1141.
Hossain, M.A., Gan, T.Y., Baki, A.B.M., 2013. Assessing morphological changes of the Ganges River using satellite images. Quat. Int. 304:142–155. https://doi.org/10.1016/j.quaint.2013.03.028.
Islam, M., Sado, K., 2000. Flood hazard assessment in Bangladesh using NOAA AVHRR data with geographical information system. Hydrol. Process. 14 (3), 605–620.
Itoh, Y., Takemura, K., Kawabata, D., Tanaka, Y., Nakaseko, K., 2001. Quaternary tectonic warping and strata formation in the southern Osaka Basin inferred from reflection seismic interpretation and borehole sequences. J. Asian Earth Sci. 20 (1), 45–58.
Jacinto, R., Grosso, N., Reis, E., Dias, L., Garrett, P., 2014. Continental Portuguese territory flood susceptibility index-contribution for a vulnerability index. Nat. Hazards Earth Syst. Sci. 2 (12), 7521–7552.
Janssen, R., Van Herwijnen, M., 1994. Multi-objective Decision Support for Environmental Management. Kluwer Academic Publishers, Dordrecht, p. 232.
Jensen, J.R., 2005. Introductory Digital Image Processing: A Remote Sensing Perspective. Prentice Hall, Toronto.
Jiang, R., Gan, T.Y., Xie, J., Ni, W., Kuo, C.C., 2015. Historical and potential changes of precipitation and temperature of Alberta subjected to climate change impact: 1900–2100. Theor. Appl. Climatol https://doi.org/10.1007/s00704-015-1664-y.
Kazakis, N., Kougias, I., Patsialis, T., 2015. Assessment of flood hazard areas at a regional scale using an index-based approach and analytical hierarchy process: application in Rhodope–Evros region, Greece. Sci. Total Environ. 538, 555–563.
Kerschgens, M.J., Drauschke, R.L., 1986. On the energy budget of a wintry mid-latitude city atmosphere. Contrib. Atmos. Phys. 59, 115–125.
La Riche, W., 1996. Alexandria: The Sunken City. Weidenfeld & Nicolson.
Lee, S., Pradhan, B., 2006. Probabilistic landslide hazards and risk mapping on Penang Island, Malaysia. J. Earth Syst. Sci. 115 (6), 661–672.
Lehner, B., Verdin, K., Jarvis, A., 2006. HydroSHEDS Technical Documentation. World Wildlife Fund US, Washington, DC available at. http://hydrosheds.cr.usgs.gov.
Lim, K.J., Engel, B.A., Muthukrishnan, S., Harbor, J., 2006. Effects of initial abstraction and urbanization on estimated runoff using CN technology. J. Am. Water Resour. Assoc. 42 (3), 629–643.
Melesse, A.M., Abtew, W. (Eds.), 2016. Landscape Dynamics, Soils and Hydrological Processes in Varied Climates. Springer International Publishing.
Moghaddam, D.D., Rezaei, M., Pourghasemi, H.R., Pourtaghie, Z.S., Pradhan, B., 2015. Groundwater spring potential mapping using bivariate statistical model and GIS in the Taleghan Watershed, Iran. Arab. J. Geosci. 8 (2), 913–929.
Nouh, M.A., 2006. Wadi flow in the Arabian Gulf states. Hydrol. Process. 20, 2393–2413.
Nyarko, B.K., 2002. Application of a rational model in GIS for flood risk assessment in Accra, Ghana. J. Spat. Hydrol. 2 (1), 1–14.
Ouma, Y.O., Tateishi, R., 2014. Urban flood vulnerability and risk mapping using integrated multi-parametric AHP and GIS: methodological overview and case study assessment. Water 6 (6), 1515–1545.
Pilgrim, D.H., Chapman, T.G., Doran, D.G., 1988. Problems of rainfall-runoff modelling in arid and semiarid regions. Hydrol. Sci. J. 33 (4), 379–400.
Pradhan, B., 2009. Flood susceptible mapping and risk area delineation using logistic regression, GIS and remote sensing. J. Spat. Hydrol. 9, 1–18.
Ramanathan, V., Crutzen, P.J., Kiehl, J.T., Rosenfeld, D., 2001. Aerosols, climate, and the hydrological cycle. Science 294, 2119–2124.
Ren, G., Zhou, Y., Chu, Z., Zhou, J., Zhang, A., Guo, J., Liu, X., 2008. Urbanization effects on observed surface air temperature trends in North China. J. Clim. 21 (6), 1333–1348.
Saaty, T.L., 1977. A scaling method for priorities in hierarchical structures. J. Math. Psychol. 15, 57–68.
Saaty, T.L., 1980. The Analytic Hierarchy Process. McGraw-Hill, New York.
Saaty, T.L., 1990. How to make a decision: the analytic hierarchy process. Eur. J. Oper. Res. 48, 9–26.
Satterthwaite, D., 2008. Climate change and urbanization: effects and implications for urban governance. United Nations Expert Group Meeting on Population Distribution, Urbanization, Internal Migration and Development, pp. 21–23.
Sen, P.K., 1968. Estimates of the regression coefficient based on Kendall's tau. J. Am. Stat. Assoc. 63, 1379–1389.
Şen, Z., 2004. Hydrograph Methods, Arid Regions. Saudi Geological Survey (SGS) (Technical Report).
Shanahan, T.M., Overpeck, J.T., Anchukaitis, K.J., Beck, J.W., Cole, J.E., Dettman, D.L., Peck, J.A., Scholz, C.A., King, J.W., 2009. Atlantic forcing of persistent drought in West Africa. Science 324, 377–380.
Shi, P.J., Yuan, Y., Zheng, J., Wang, J.A., Ge, Y., Qiu, G.Y., 2007. The effect of land use/cover change on surface runoff in Shenzhen region, China. Catena 69 (1), 31–35.
Tehrany, M.S., Pradhan, B., Jebur, M.N., 2013. Spatial prediction of flood susceptible areas using rule based decision tree (DT) and a novel ensemble bivariate and multivariate statistical models in GIS. J. Hydrol. 504, 69–79.
Tehrany, M.S., Pradhan, B., Mansor, S., Ahmad, N., 2015. Flood susceptibility assessment using GIS-based support vector machine model with different kernel types. Catena 125, 91–101.
Termeh, S.V.R., Kornejady, A., Pourghasemi, H.R., Keesstra, S., 2018. Flood susceptibility mapping using novel ensembles of adaptive neuro fuzzy inference system and metaheuristic algorithms. Sci. Total Environ. 615, 438–451.
Wang, X.L., Wen, Q.H., Wu, Y., 2007. Penalized maximal t test for detecting undocumented mean change in climate data series. J. Appl. Meteorol. Climatol. 46 (6), 916–931.
Wijngaard, J.B., Klein Tank, A.M.G., Können, G.P., 2003. Homogeneity of 20th century European daily temperature and precipitation series. Int. J. Climatol. 23 (6), 679–692.
Williams, A., Funk, C., 2011. A westward extension of the warm pool leads to a westward extension of the Walker circulation drying eastern Africa. Clim. Dyn. 1–19.
Xiao, Y., Yi, S., Tang, Z., 2017. Integrated flood hazard assessment based on spatial ordered weighted averaging method considering spatial heterogeneity of risk preference. Sci. Total Environ. 599, 1034.
Xu, Q., Dong, Y.X., Yang, R., 2018. Urbanization impact on carbon emissions in the Pearl River Delta region: Kuznets curve relationships. J. Clean. Prod. 180, 514–523.
Yan, Z., Li, Z., Jones, P., 2010. Effects of site change and urbanisation in the Beijing temperature series 1977–2006. Int. J. Climatol. 30 (8), 1226–1234.
Zhan, X., Huang, M.L., 2004. ArcCN-runoff: an ArcGIS tool for generating curve number and runoff maps. Environ. Model. Softw. 19 (10), 875–879.
Zhang, H., Ma, W.C., Wang, X.R., 2008a. Rapid urbanization and implications for flood risk management in hinterland of the Pearl River Delta, China: the Foshan study. Sensors 8 (4), 2223–2239.
Zhang, Q., Xu, C.Y., Zhang, Z., Chen, Y.D., Liu, C.L., Lin, H., 2008b. Spatial and temporal variability of precipitation maxima during 1960–2005 in the Yangtze River basin and possible association with large-scale circulation. J. Hydrol. 353 (3), 215–227.
Zhao, G., Pang, B., Xu, Z., Yue, J., Tu, T., 2018. Mapping flood susceptibility in mountainous areas on a national scale in China. Sci. Total Environ. 615, 1133–1142.